Non-reciprocal Transmission of Vibrational Energy in a Locally Resonant Elastic Metabeam

M. A. Attarzadeh[a,b], J. Callanan[a,b], M. Nouh[a,b,*]

[a]*Sound and Vibrations Laboratory, University at Buffalo (SUNY), Buffalo, NY 14260, USA*

[b]*Dept. of Mechanical and Aerospace Engineering, University at Buffalo (SUNY), Buffalo, NY 14260, USA*

Abstract

Despite the promising theoretical outcomes of spatiotemporally modulated phononic crystals and metamaterials in one-way isolation of elastic waves, limited success has been achieved in obtaining a feasible magnet-free realization of the concept for real-world applications. This work entails the design and operation of a vibration diode which exploits the inherent geometric-dependence of stiffness in non-axisymmetric cross sections. The diode relies on a phase shift between the geometric orientations of an array of resonators attached to a host beam to prescribe a spatial modulation of the metamaterial stiffness, accompanied with a uniform rotation induced via small motor action to effectively onset a spatiotemporal stiffness profile. The proposed configuration capitalizes on the simple design and versatility of locally resonant elastic metabeams (EMs) and can, therefore, be tailored to different application requirements without interfering with the primary functions and structural requirements of the main system. Both theoretical and numerical tools have been incorporated to prove the effectiveness of the proposed system in one-way isolation of mechanical vibrations. Preliminary results pertaining to the experimental setup of the diode are also outlined. The study aims to lay a forward path for micro/macro-scale implementation of linear vibration diodes.

1. Introduction

The mechanics of wave propagation in elastic solids have been thoroughly investigated over the past few decades [1–4]. Motivated by their unique wave manipulation capabilities, periodic structures exhibiting tunable band gaps, directional wave guidance, and negative effective densities have culminated in a spurt of research efforts [5–8]. Most recently, in pursuit of new functionalities, novel configurations have been presented as pathways to break elastic wave reciprocity and onset a diode-like behavior [9], as well as logical gates in the mechanical domain [10]. Materials with properties that vary simultaneously in space and time have

*Corresponding author:
Email address: mnouh@buffalo.edu (M. Nouh)

been the focus of a number of efforts to investigate wave amplification and non-reciprocity in linear systems [11, 12]. In theory, a vibrating structure which comprises time-dependent elastic components is no longer bound by the reciprocal constraints [13], and such problem has been recently investigated in the context of one- [14] and two-dimensional [15] structures using the Plane Wave Expansion Method (PWEM). Additionally, non-reciprocal waves have been recently reported in elastic metabeams (EMs) [16] and locally resonant systems [17, 18]. Such EMs typically comprise a continuous beam attached to an array of mechanical resonators, and a non-reciprocal behavior is onset following a temporal modulation of the elastic properties of the host beam, the resonators, or both in a traveling-wave-like manner [17]. Various ideas have been proposed to induce such modulations including the use of a moving train of light beams on a photoelastic material [19], voltage-controlled piezoelectric patches [20], as well as a traveling magnetic field imposed on a magnetoelastic material [21]. While all are valiant efforts, the need for hard-wired setups and complex experimental configurations pose legitimate concerns pertaining to practicality as well as ease of operation.

In this effort, we introduce a magnet-free design of a sub-wavelength mechanical diode that incorporates space-time variation of resonator geometry. The proposed system relies on breaking time-reversal symmetry by inducing an artificial traveling-wave-like variation of the resonators' stiffness to achieve the non-reciprocal behavior. Instead of relying on smart and electromechanically coupled materials, we employ a design which utilizes synchronized rotations of the resonator array to induce geometric stiffness modulations along the length of the EM. In addition to the breakage of wave propagation symmetry, the proposed vibration diode inherits the tunability of frequency band gaps in conventional EMs, which in turn extends the non-reciprocal behavior to lower frequencies. The rest of this paper is arranged in a way to provide insights on the operational principle of the diode, followed by a dynamic analysis (both theoretical and numerical) to illustrate the breakage of reciprocal symmetry, and finally a description of the proposed experimental testing which is currently underway.

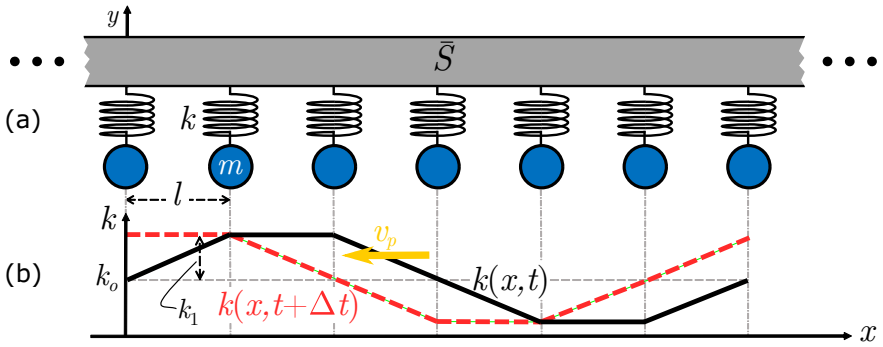

Figure 1 Schematic of an elastic metabeam (EM): (a) A host beam with a bending stiffness $\bar{S}$ attached to an array of resonators, each consisting of a spring k and a tip mass of m. (b) The space-time-periodic variation of the stiffness analogous to a wave traveling with velocity v_p in the opposite x-direction.

2. Operational Principle

The first step in the vibrational diode design is the build-up and operation of a conventional Elastic Metabeam (EM). Fig. 1a shows the configuration of an EM beam which consists of a host structure (a homogeneous beam with bending stiffness $\bar{S}$), which is attached to a number of resonators with mass m and spring stiffness k, equally spaced at a distance l. The band gap frequency range primarily depends on the resonator mass and stiffness and can therefore appear at relatively low frequencies – potentially even on the order of ten or one hundred hertz [22]. In conventional EMs, the emergent band gap will remain indifferent to the propagation direction of the elastic waves due to the reciprocity principle. Such reciprocity can be broken by incorporating a traveling-wave-like modulation of the resonator stiffness to induce an artificial directional bias. Hereafter, we focus on the objective of creating a k-profile which varies both spatially and temporally to follow a wave traveling with velocity v_p along the length of the beam, as shown in Fig. 1b. Consider an apparatus where a series of resonators, each comprising a heavy tip mass and a lightweight arm, are attached to both sides of a host beam as shown in Fig. 2. As a result, the resonator stiffness k is equal to the arm's lateral stiffness in the y-direction. For an isotropic prismatic beam under the Euler-Bernoulli theory, the lateral stiffness of the arm is given by

$$k = \frac{3EI_x}{l_a^3} \tag{1}$$

where E, I_x, and l_a are the elastic modulus, area moment of inertia, and the length of the arm, respectively. As can be inferred from Eq. (1), the stiffness constant of the arm can be regulated by changing either its geometry (and thus I_x) or its material (and thus E). Effective and instantaneous control of material properties requires active materials with electromechanical coupling. Instead, controlling the geometry (with respect to the transverse vibration direction) provides a viable and a cost-efficient way to achieve the required stiffness modulations. The area moment of inertia for the arm cross section in the x-y plane is

$$I_x = \int_A y^2 \, dA \tag{2}$$

For a circular cross section, I_x remains unchanged with an arbitrary rotation about the z-axis due to its axisymmetry. For an ellipse or a rectangle, however, this will no longer be the case. Let x' and y' be the principal axes for the arm cross sectional area and θ be the clockwise angular orientation of x with respect to x'. Following the coordinate rotation principle, we get

$$I_x = I_o + I_1 \cos(2\theta) \tag{3}$$

where $I_o = \frac{I_{x'}+I_{y'}}{2}$ and $I_1 = \frac{I_{x'}-I_{y'}}{2}$. Eq. (3) implies that different orientations of the arm

about the z-axis will result in different values of I_{ax} if $I_{x'} \neq I_{y'}$. Furthermore, a rotation of the arm about the z-axis will induce a harmonically changing I_x with a period of π.

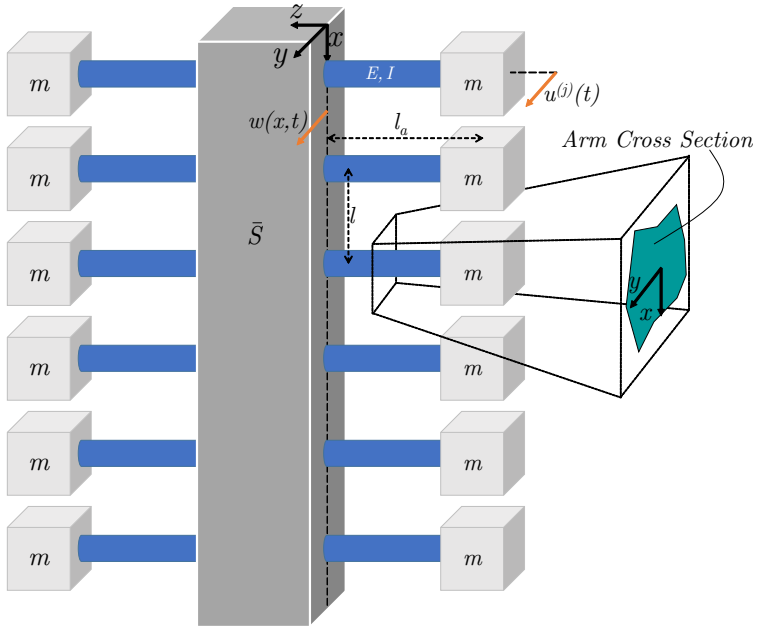

Figure 2 Proposed elastic metabeam setup with resonators extending from both sides of the host beam for symmetry. Spring stiffness of the resonators emerge from lateral deflection of the resonator arms in the y-direction, which in turn is a function of the area moment of inertia of the cross section.

To validate such variation of the resonator stiffness with rotations about z-axis, a set of numerical simulations are carried out for an arm with various rectangular cross sections. Fig. 3 shows the stiffness variation with respect to the rotation angle for the cross sectional ratios of $r = 0.25$, 0.5, 0.9 and 1, with the cross section kept at 0.175 in^2. The stiffness variation vanishes at $r = 1$ as anticipated. In addition, for lower cross sectional ratios, the modulation amplitude is greater, as suggested by Eq. (3). It is also worth noting that at higher r, the variation does not follow a harmonic function, but rather exhibits wider valleys. This effect can be attributed to the limitations of Euler-Bernoulli beam formulation.

Accordingly, three possible stiffness modulation scenarios can be devised. First, an angular phase shift between the orientation of adjacent arms with rectangular cross sections is prescribed. The spatial variation of the spring constants k along the beam's length is approximately given by

$$k^{(j)} = k_o + k_1 \cos(2\phi_j) \tag{4}$$

where $j = 1, 2, ...J$ is the resonator index inside each super cell, k_o and k_1 are the average and alternating parts of the spring constants, respectively, and $\phi_j = \pi j/J$ is the angular orientation of the j^{th} arm, with J being the total number of unit cells per super cell.

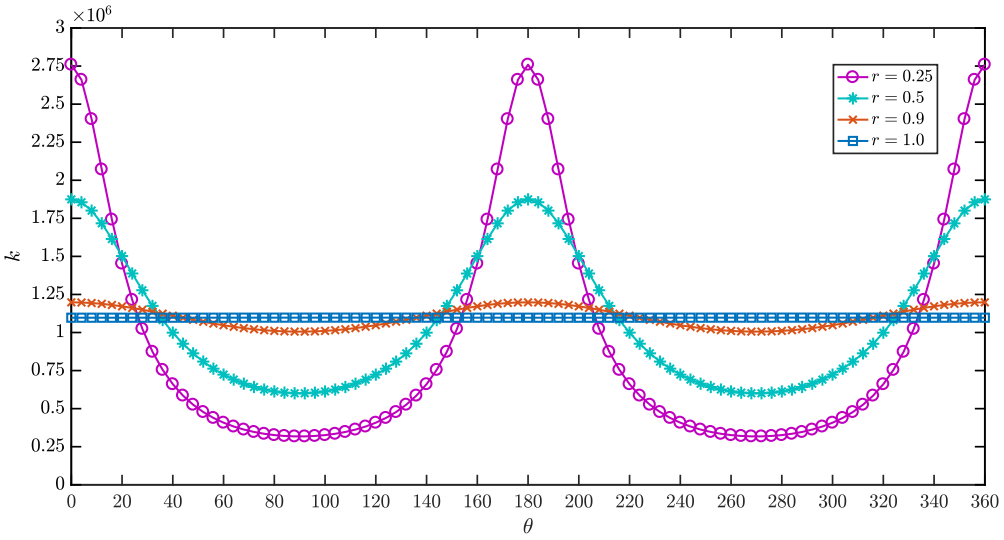

Figure 3 Variation of resonator stiffness for a rectangular cross section with different aspect ratios r.

In the second scenario, we align all the rectangular arms and start rotating them with a constant angular frequency ω_e provided by a set of electric motors. As a result, $\theta_j = \omega_e t$ and consequently the resonators' stiffness will be identical but temporally periodic, i.e.

$$k(t) = k_o + k_1 \cos(2\omega_e t) \tag{5}$$

In the third and last scenario, we combine the two previous cases to achieve a simultaneous spatial and temporal modulation of the resonators elastic properties. In other words, each resonator arm is oriented with a phase shift with respect to the adjacent resonator in addition to being continuously rotated with the prescribed angular frequency ω_e, which yields

$$k^{(j)}(t) = k_o + k_1 \cos(2\omega_e t + 2\phi_j) \tag{6}$$

In this case an effective variation of resonators' stiffness is induced that follows a traveling wave function. As a result breakage of reciprocal symmetry can take place as will be detailed in the next section.

3. Dynamic Analysis

3.1. Wave propagation and dispersion diagrams

In the long wavelength regime, a traveling-wave-like stiffness variation of resonators along the EM beam, i.e. Eq. (6), can be replaced by a continuous function of space x and time t

$$k(x,t) = k_o + k_1 \cos(\omega_p t + \kappa_p x) \tag{7}$$

where, $\kappa_p = \frac{2\pi}{Jl}$ is the spatial modulation frequency and $\omega_p = 2\omega_e$ is the temporal pumping frequency. Thus, the traveling velocity of the pumped stiffness is $v_p = \frac{-\omega_p}{\kappa_p}$, similar to a wave traveling in the opposite direction of the x-axis (see Fig. 1). As such, displacement of spatially discrete resonators $u^{(j)}(t)$ can also be replaced by a continuous function $u(x,t)$. Therefore, the lateral dynamics, $w(x,t)$ of a locally resonant metabeam with a bending stiffness $\bar{S}$, and mass per unit length $\bar{\mu}$ is governed by the following motion equations:

$$\bar{S}\frac{\partial^4 w}{\partial x^4} + \bar{\mu}\frac{\partial^2 w}{\partial t^2} = \frac{1}{l}k(x,t)(u-w) \tag{8a}$$

$$m\frac{\partial^2 u}{\partial t^2} = k(x,t)(w-u) \tag{8b}$$

To overcome the complexities associated with the time-varying nature of Eq. (8), for the purposes of the dispersion analysis, we study elastic waves in the same metabeam while it is simultaneously moving in the positive direction of the x-axis with a velocity of $v = \frac{\omega_p}{\kappa_p}$. This way, time-modulation of the properties will no longer be detectable to a stationary observers [23]. As such, by adding the Coriolis and Centripetal terms arising from actual motion of the beam, Eq. (8) becomes

$$S\frac{\partial^4 w}{\partial x^4} + \mu\left(\frac{\partial^2 w}{\partial t^2} + 2v\frac{\partial^2 w}{\partial t \partial x} + v^2\frac{\partial^2 w}{\partial x^2}\right) = k(x)(u-w) \tag{9a}$$

$$m\left(\frac{\partial^2 u}{\partial t^2} + 2v\frac{\partial^2 u}{\partial t \partial x} + v^2\frac{\partial^2 u}{\partial x^2}\right) = k(x)(w-u) \tag{9b}$$

where $S = \bar{S}l$ and $\mu = \bar{\mu}l$. Eq. (9) describes lateral deformations of a metabeam moving in the x-direction while its resonators encounter a stiffness modulation traveling with the same speed but in the opposite direction. As anticipated, the actual motion of the beam nullifies the artificial traveling-wave of the resonator properties and the time-varying problem simplifies to time-invariant one with resonators' stiffness only a function of space, i.e. $k(x) = k_o + k_1\cos(\kappa_p x)$. Subsequently, the Coriolis terms ($2v\frac{\partial^2 w}{\partial t \partial x}$ and $2v\frac{\partial^2 u}{\partial t \partial x}$) now carry the directional bias, instead. Let us now assume plane wave solutions for both w and u in Eq. (9) with frequency ω and wavenumber κ. This results in

$$[\kappa^4 S + k_o - \mu(\omega - \kappa v)^2]W - k_o U + \frac{k_1}{2}(W_{+1} + W_{-1} - U_{+1} - U_{-1}) = 0 \tag{10a}$$

$$[k_o - m(\omega - \kappa v)^2]U - k_o W - \frac{k_1}{2}(W_{+1} + W_{-1} - U_{+1} - U_{-1}) = 0 \tag{10b}$$

where U and W are the harmonic wave amplitudes while $W_{\pm 1}$ and $U_{\pm 1}$ are short hand notations for $W(\kappa \pm \kappa_p)$ and $U(\kappa \pm \kappa_p)$, respectively. Using Eq. (10), it can be shown that

the amplitude of waves traveling in the resonators are related to the amplitude of waves traveling in the beam by

$$U = \frac{\kappa^4 S - \mu(\omega - \kappa v)^2}{m(\omega - \kappa v)^2} W \tag{11}$$

which, upon substitution in Eq. (10)a, results in

$$aW + b_{+1}W_{+1} + b_{-1}W_{-1} = 0 \tag{12}$$

where

$$a(\omega, \kappa) = \kappa^4 S - \mu(\omega - \kappa v)^2 + k_o \left(1 - \frac{\kappa^4 S - \mu(\omega - \kappa v)^2}{m(\omega - \kappa v)^2}\right) \tag{13a}$$

$$b(\omega, \kappa) = \frac{k_1}{2} \left(1 - \frac{\kappa^4 S - \mu(\omega - \kappa v)^2}{m(\omega - \kappa v)^2}\right) \tag{13b}$$

are explicit functions of ω and κ. The terms with $W_{\pm 1}$ carry the effects of the stiffness modulation. Therefore, a zero$^{\text{th}}$ order approximation of the dispersion behavior, obtained by neglecting such terms as $a(\omega, \kappa) = 0$, will not be affected by the modulation of resonators. On the other hand, a first-order approximation requires using the recursive nature of Eq. (12). As such, we can write

$$a_{+1}W_{+1} + b_{+2}W_{+2} + bW = 0 \tag{14a}$$

$$a_{-1}W_{-1} + bW + b_{-2}W_{-2} = 0 \tag{14b}$$

by up- and down-shifting the wavenumber by an amount κ_p. Neglecting terms with higher than the first harmonic in Eq. (14) gives $W_{+1} = \frac{-b}{a_{+1}} W$ and $W_{-1} = \frac{-b}{a_{-1}} W$ which, after substituting back in Eq. (12), leads to

$$a - b\left(\frac{b_{+1}}{a_{+1}} + \frac{b_{-1}}{a_{-1}}\right) = 0 \tag{15}$$

As shown in the Eq. (15), incorporating amplitude of the waves with $\kappa \pm \kappa_p$ wavenumbers results in corrections made to the zero$^{\text{th}}$ order dispersion relation. Derivation of a higher-order approximation is similarly straight forward. Refer to Appendix I for second-order and third-order dispersion relations. The dispersion patterns of the zero$^{\text{th}}$, first, and third order approximations for a moving metabeam with space-time periodic resonator stiffness are compared in Figs. 4a through c. As apparent, higher order approximations exhibit extra

dispersion bands and thus more accurate dynamics. It is, however, more customary to use a first-order approximation due to the inconsequential contributions from higher harmonics. The asymmetrical group velocities on both sides of the ω axis in Fig. 4a-c are reminiscent of the drag effect observed in moving media [23]. In addition, as previously discussed, the actual motion of the beam cancels out the non-reciprocity arisen from space-time periodic stiffness variation. As such, band gaps are located at the same frequency ranges on both sides of the ω axis.

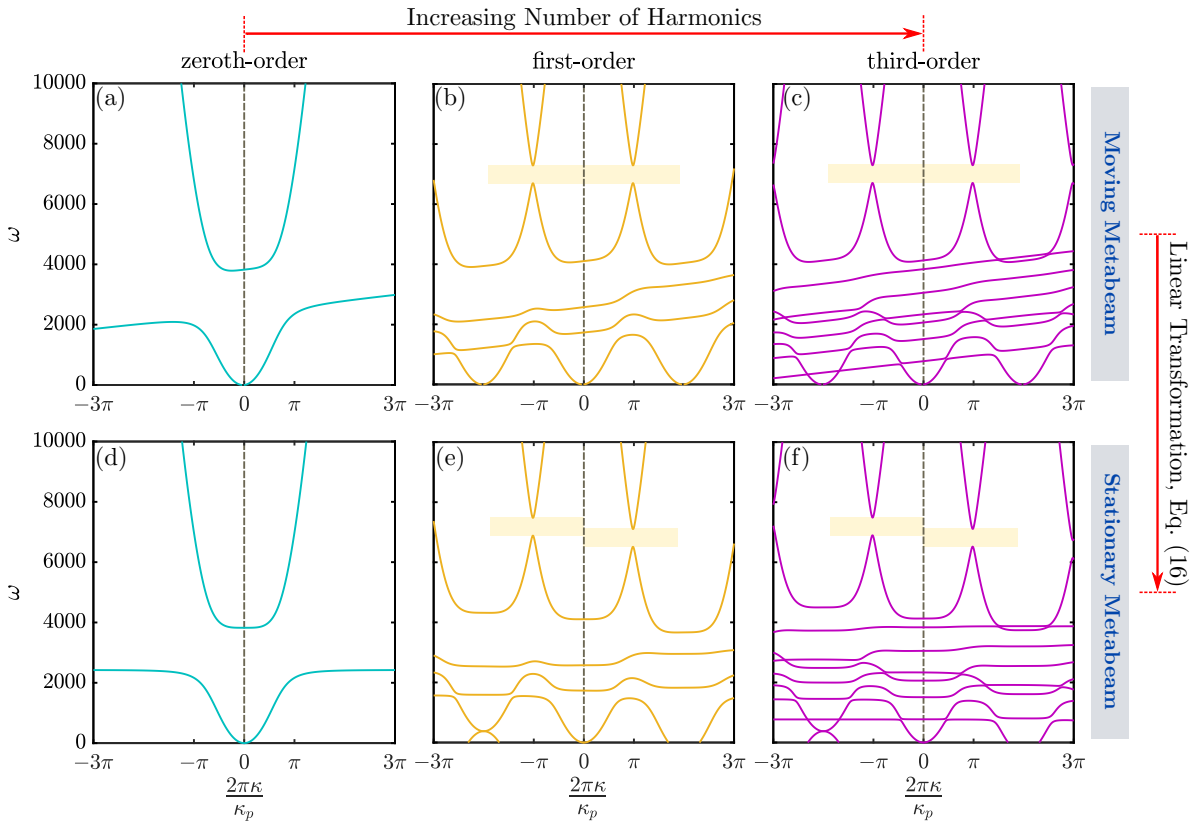

Figure 4 Dispersion diagrams for a non-reciprocal metabeam with 4 unit cells per super cell. Parameters are: $S = 30.2555$ N.m^3 , $\mu = 0.1143$ kg, $m = 0.17$ kg, $k_0 = 1e6$ N/m, $k_1 = 0.75k_0$, and $v = 9.6317$ m/s. (a), (b) and (c) represent the zeroth, first and third order solutions of the dispersion relation for a moving EM, respectively. (d), (e) and (f) represent the corresponding dispersion diagrams for a stationary EM.

Eventually, the last step towards obtaining the dispersion plots of a stationary space-time periodic metabeam (the original problem) is to nullify the initially added moving velocity in the energy-momentum space. This is achieved by incorporating a linear coordinate transformation matrix given by

$$\begin{bmatrix} \kappa \\ \omega \end{bmatrix}_{\mathbf{S}} = \begin{bmatrix} 1 & 0 \\ -v & 1 \end{bmatrix} \begin{bmatrix} \kappa \\ \omega \end{bmatrix}_{\mathbf{M}} \tag{16}$$

The subscripts **S** and **M** denote stationary and moving systems, respectively. The imple-

mentation of such vertical shear transformation restores the dispersion plots of the space-time-periodic EM as shown in Figs. 4d-f revealing the broken and asymmetric band gaps.

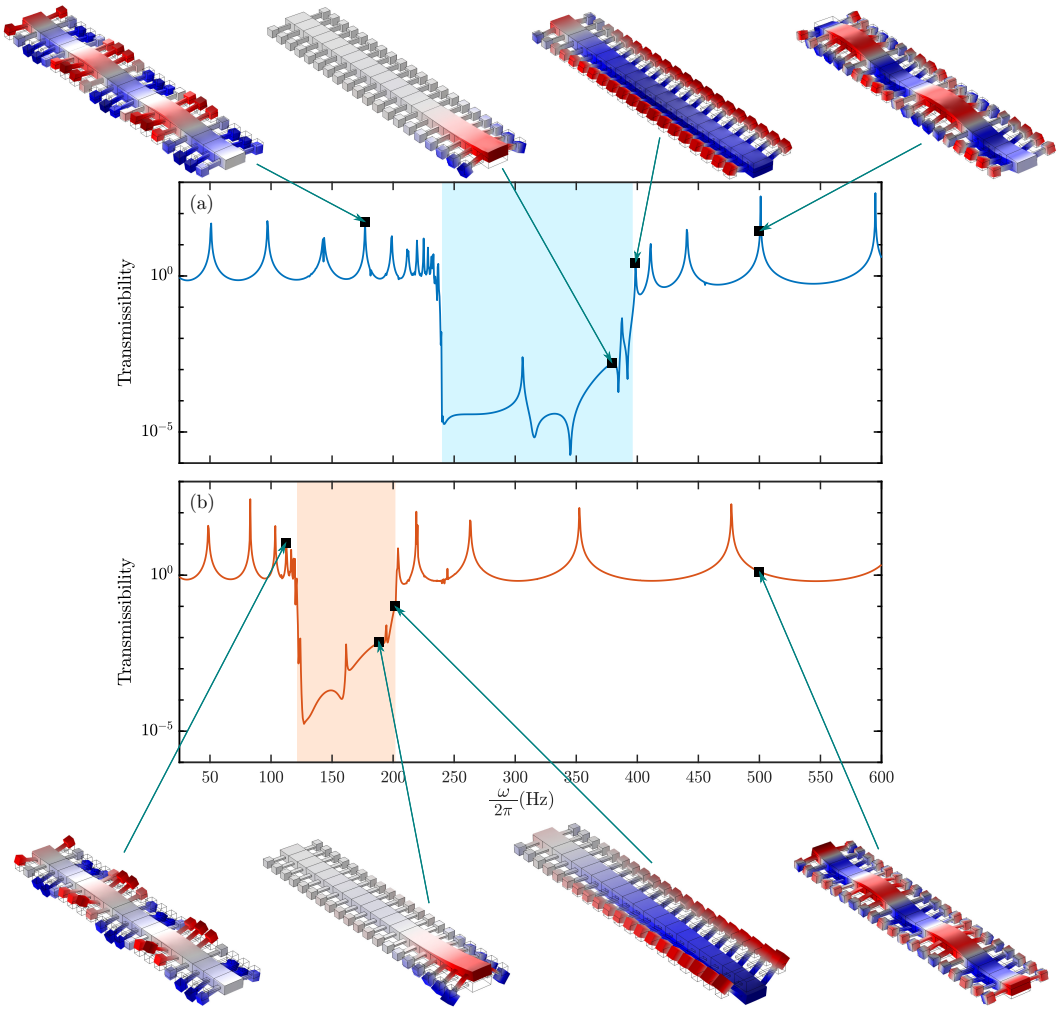

Figure 5 Transmissibility frequency response plots for an elastic metabeam (EM) with the orientation of the resonator arms set to: (a) $\theta = 0^{\circ}$ (*highest stiffness*) and (b) $\theta = 90^{\circ}$ (*lowest stiffness*).

3.2. Finite Element Analysis

In order to obtain an estimate for the band gap frequency ranges of the proposed metamaterial beam configuration, a set of finite element numerical studies are carried out. COMSOL multi-physics is employed to solve a frequency response problem of a metabeam with twenty resonators on each side. A harmonic force is imparted on one side of the metabeam and its lateral vibration is measured on the other side. The main beam is assumed to be made of ABS plastic with $\bar{\mu} = 2.849$ kg/m and $\bar{S} = 754.23$ N.m^2 for a relatively slow wave propagation speed. The resonator arms are considered to be made of aluminum and the tip masses

made of steel. The arm's cross sectional ratio is $r = 0.448$, its cross sectional area is 0.175 in^2 and its length is 2 inches. The tip masses are sized to have a weight of 6 oz.

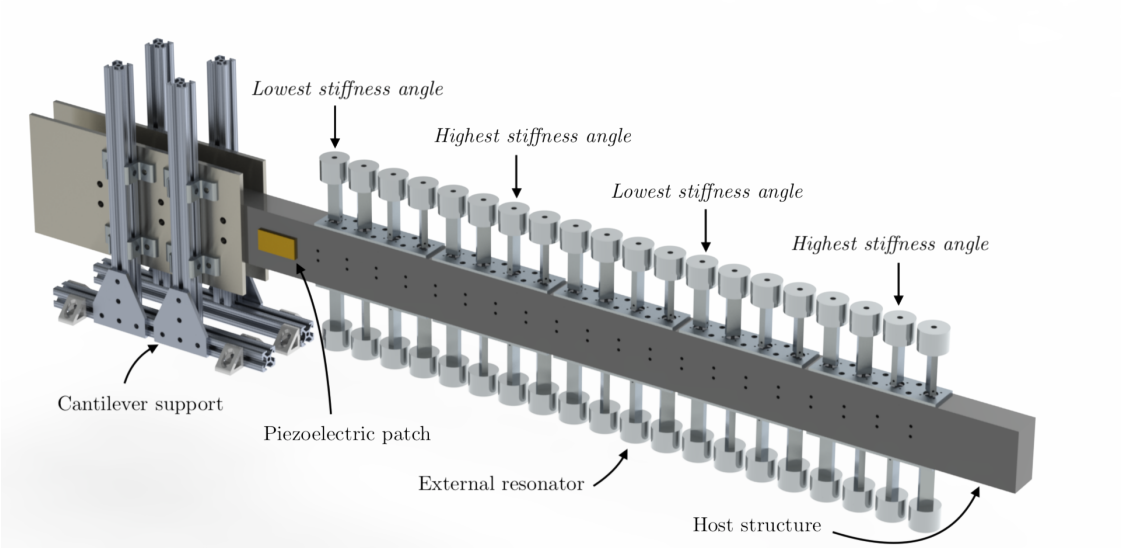

Figure 6 Experimental vibration diode apparatus.

Fig. 5a shows frequency response of the metabeam when its resonators are oriented at $\theta = 0^{\text{o}}$, corresponding to the highest lateral stiffness of the arms. The band gap frequency range appears to span a wide range of 240 to 395 Hz. On the other hand, for the lowest stiffness (obtained after rotating resonators by 90^{o}), Fig. 5b shows a completely different band gap range spanning the frequency range $125 < \omega < 200$ Hz.

4. Experimental Setup

The experimental apparatus of the EM is shown in Fig. 6. The metabeam consists of a base or host structure and external resonators. The resonators are fixed to stepper motors that are embedded within the host beam itself. Fig. 6 shows a snapshot in time where the resonators exhibit a spatial variation in stiffness. The resonator arms have a width-to-length-to-height ratio of $1 : 2.23 : 7.14$. The resonator arm closest to the cantilever support has the least possible second moment of area of this configuration. The spatial stiffness variation arises from a change in angle of the resonator arm with respect to the vibration direction: each resonator arm is rotated by 45^{o} with respect to the previous one, and consequently every other resonator arm has either the maximum or minimum possible stiffness. The impact of the change in stiffness of the resonator arms on the host structure is maximized by incorporating a tip mass resonator onto each resonator arm. The arms are machined from 6061 aluminum and the tip masses are low-carbon steel. Fig. 7a shows the full-scale assembled experimental device and Fig. 7b shows an exploded view of one set of tip masses, resonator arms, face plate, and motors. The face plate is used to secure the

motors to the host structure. The motors can be controlled independently or synchronized to achieve any type of spatiotemporal stiffness modulation.

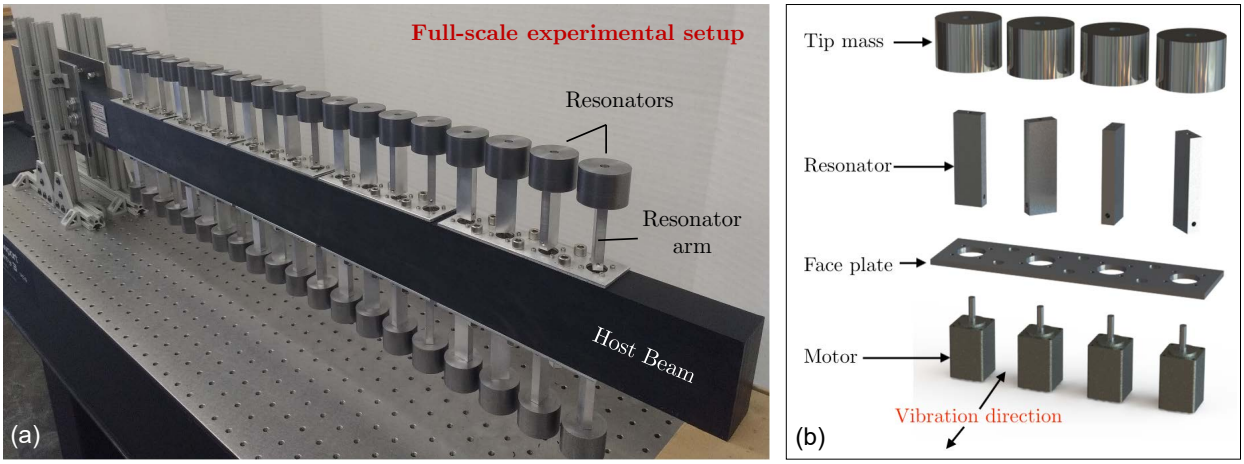

Figure 7 Exploded view showing motors, face plate, resonator arms, and tip masses.

The central performance requirement of the proposed apparatus is that the change stiffness of the resonator must have a significant impact on the host structure. Fig. 8a shows a test fixture made to secure a NEMA 14 stepper motor to an electrodynamic shaker. Two accelerometers were used to find the transfer function between the motion of the tip mass and the motion of the shaker fixture. The test results are shown in Fig. 8b. A sine-sweep of the shaker excitation frequency reveals the natural frequencies of the resonator arm and motor system. We observe that for low frequencies, the high- and low-stiffness configurations are almost indistinguishable. In the vicinity of 1 kHz, however, the frequency response functions show peaks at different locations. This basic verification of the change in natural frequency (and therefore stiffness) of the mass-beam-motor system confirms the potential for harnessing this effect to realize a spatiotemporal stiffness modulation in a host structure.

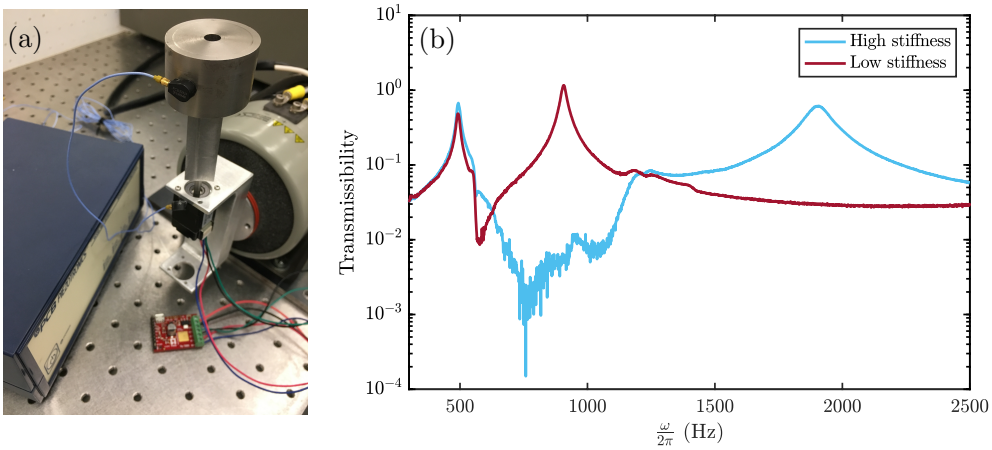

Figure 8 Experimental verification of in resonance frequency variation under rotation.

5. Conclusions

This paper has presented the operational concept and early experimental build-up of a vibrational diode based on a locally resonant elastic metabeam (EM). In its operation, the non-reciprocal EM consists of a host beam attached to a set of configurable miniature cantilever resonators. A prescribed phase shift between the geometric orientations of the resonators within each unit cell results in a predictable spatial elastic profile. The resonators are then rotated by a set of driven motors to introduce a concurrent uniform temporal variation across the entire device. The combined spatiotemporal modulation of the resonators elastic properties breaks the dispersion symmetry and induces two distinct frequency band gaps depending on the propagation direction. As a result, excitations falling within the spectrum of each band gap onsets a diode-like unidirectional transmission of energy and, consequently, a non-reciprocal behavior. The modeling of the proposed metabeam is outlined and is followed by a characterization of its performance including a dispersion and a vibration transmissibility analysis. The design and assembly of the device are highlighted and experimental testing of its performance is currently underway.

Acknowledgments

Support of this work from the Vibration Institute through its academic grant program is greatly acknowledged.

Appendix I: Higher order dispersion relations of the Non-reciprocal metabeam with contributions from second and third harmonics

By following a procedure similar to that of Eq. (12) to Eq. (15), the second-order dispersion relation can be found as

$$a - b\left(\frac{b_{+1}}{a_{+1} - b_{+1}\frac{b_{+2}}{a_{+2}}} + \frac{b_{-1}}{a_{-1} + b_{-1}\frac{b_{-2}}{a_{-2}}}\right) = 0 \tag{17}$$

and the third order dispersion relation as

$$a - b\left(\frac{b_{+1}}{a_{+1} - b_{+1}\frac{b_{+2}}{a_{+2} - b_{+2}\frac{b_{+3}}{a_{+3}}}} + \frac{b_{-1}}{a_{-1} - b_{-1}\frac{b_{-2}}{a_{-2} - b_{-2}\frac{b_{-3}}{a_{-3}}}}\right) = 0 \tag{18}$$

References

[1] J. F. Doyle, Wave propagation in structures, in: Wave Propagation in Structures, Springer, 1989, pp. 126–156.

[2] L. Brillouin, Wave propagation in periodic structures: electric filters and crystal lattices, Courier Corporation, 2003.

[3] D. Mead, Wave propagation in continuous periodic structures: research contributions from southampton, 1964–1995, Journal of sound and vibration 190 (3) (1996) 495–524.

[4] M. I. Hussein, M. J. Leamy, M. Ruzzene, Dynamics of Phononic Materials and Structures: Historical Origins, Recent Progress, and Future Outlook, Applied Mechanics Reviews 66 (4) (2014) 040802. doi:10.1115/1.4026911.

[5] P. Celli, S. Gonella, Tunable directivity in metamaterials with reconfigurable cell symmetry, Applied Physics Letters 106 (9). doi:10.1063/1.4914011.

[6] Y. Chen, G. Huang, C. Sun, Band gap control in an active elastic metamaterial with negative capacitance piezoelectric shunting, Journal of Vibration and Acoustics 136 (6) (2014) 061008.

[7] H. H. Huang, C. T. Sun, G. L. Huang, On the negative effective mass density in acoustic metamaterials, International Journal of Engineering Science 47 (4) (2009) 610–617.

[8] M. Nouh, O. Aldraihem, A. Baz, Periodic metamaterial plates with smart tunable local resonators, Journal of Intelligent Material Systems and Structures 27 (13) (2016) 1829–1845.

[9] M. B. Zanjani, A. R. Davoyan, A. M. Mahmoud, N. Engheta, J. R. Lukes, One-way phonon isolation in acoustic waveguides, Applied Physics Letters 104 (8) (2014) 081905.

[10] O. R. Bilal, A. Foehr, C. Daraio, Bistable metamaterial for switching and cascading elastic vibrations, Proceedings of the National Academy of Sciences 114 (18) (2017) 4603–4606.

[11] A. Cullen, A travelling-wave parametric amplifier, Nature 181 (4605) (1958) 332.

[12] E. Cassedy, A. Oliner, Dispersion relations in time-space periodic media: Part i, stable interactions, Proceedings of the IEEE 51 (10) (1963) 1342–1359.

[13] J. Achenbach, Wave propagation in elastic solids, Vol. 16, Elsevier, 2012.

[14] G. Trainiti, M. Ruzzene, Non-reciprocal elastic wave propagation in spatiotemporal periodic structures, New Journal of Physics 18 (8) (2016) 083047.

[15] M. Attarzadeh, M. Nouh, Non-reciprocal elastic wave propagation in 2d phononic membranes with spatiotemporally varying material properties, Journal of Sound and Vibration 422 (2018) 264–277.

[16] H. Nassar, H. Chen, A. Norris, G. Huang, Non-reciprocal flexural wave propagation in a modulated metabeam, Extreme Mechanics Letters 15 (2017) 97–102.

[17] M. Attarzadeh, H. Al Babaa, M. Nouh, On the wave dispersion and non-reciprocal power flow in space-time traveling acoustic metamaterials, Applied Acoustics 133 (2018) 210–214.

[18] H. Nassar, H. Chen, A. Norris, M. Haberman, G. Huang, Non-reciprocal wave propagation in modulated elastic metamaterials, in: Proc. R. Soc. A, Vol. 473, The Royal Society, 2017, p. 20170188.

[19] N. Swinteck, S. Matsuo, K. Runge, J. Vasseur, P. Lucas, P. Deymier, Bulk elastic waves with unidirectional backscattering-immune topological states in a time-dependent superlattice, Journal of Applied Physics 118 (6) (2015) 063103.

[20] C. Croënne, J. Vasseur, O. Bou Matar, M.-F. Ponge, P. Deymier, A.-C. Hladky-Hennion, B. Dubus, Brillouin scattering-like effect and non-reciprocal propagation of elastic waves due to spatio-temporal modulation of electrical boundary conditions in piezoelectric media, Applied Physics Letters 110 (6) (2017) 061901.

[21] M. Ansari, M. Attarzadeh, M. Nouh, M. A. Karami, Application of magnetoelastic materials in spatiotemporally modulated phononic crystals for nonreciprocal wave propagation, Smart Materials and Structures 27 (1) (2017) 015030.

[22] H. Al Ba'ba'a, M. Nouh, T. Singh, Formation of local resonance band gaps in finite acoustic metamaterials: A closed-form transfer function model, Sound and Vibration Journal 410 (2017) 429 – 446.

[23] M. Attarzadeh, M. Nouh, Elastic wave propagation in moving phononic crystals and correlations with stationary spatiotemporally modulated systems, AIP Advances 8 (10) (2018) 105302.